Development 129, 2807-2822 (2002)
Printed in Great Britain © The Company of Biologists Limited 2002
DEV2789

Fate map of the chicken neural plate at stage 4

Pedro Fernández-Garre[1,*], Lucia Rodríguez-Gallardo[2,*], Victoria Gallego-Díaz[2], Ignacio S. Alvarez[2] and Luis Puelles[1,†]

[1]Department of Morphological Sciences, Faculty of Medicine, University of Murcia, 30100, Murcia, Spain
[2]Department of Cell Biology, Faculty of Sciences, University of Extremadura, 06071, Badajoz, Spain
*These authors contributed equally to this work
†Author for correspondence (e-mail: puelles@um.es)

Accepted 25 March 2002

SUMMARY

A detailed fate map was obtained for the early chick neural plate (stages 3d/4). Numerous overlapping plug grafts were performed upon New-cultured chick embryos, using fixable carboxyfluorescein diacetate succinimidyl ester to label donor chick tissue. The specimens were harvested 24 hours after grafting and reached in most cases stages 9-11 (early neural tube). The label was detected immunocytochemically in wholemounts, and cross-sections were later obtained. The positions of the graft-derived cells were classified first into sets of purely neural, purely non-neural and mixed grafts. Comparisons between these sets established the neural plate boundary at stages 3d/4. Further analysis categorized graft contributions to anteroposterior and dorsoventral subdivisions of the early neural tube, including data on the floor plate and the eye field. The rostral boundary of the neural plate was contained within the earliest expression domain of the *Ganf* gene, and the overall shape of the neural plate was contrasted and discussed with regard to the expression patterns of the genes *Plato*, *Sox2*, *Otx2* and *Dlx5* (and others reported in the literature) at stages 3d/4.

Key words: Neural plate, Fate map, Neural genes, Non-neural epiblast, Neural tube, Chick

INTRODUCTION

There is currently much interest on forebrain patterning in vertebrates. Fate maps obtained at appropriate early stages provide a background for specification maps and guide interpretation of mRNA or protein expression patterns, in order to understand gene functions and develop causal hypotheses.

We present a detailed fate map of the initial stages of neural plate formation in the chick, which may aid experimental studies on potential forebrain organizer regions. The chick neural plate has been fate-mapped several times (see Discussion). In these studies the epiblast was sampled experimentally only partially, using diverse methods [see comments by Hatada and Stern (Hatada and Stern, 1994)]. This could explain several inconsistencies regarding the existence of post-nodal prospective neuroepithelium, and the vague definition of the boundaries of the prospective neural plate (nodo-neural, neuro-epidermal and neuro-mesodermal limits), and of prospective rostrocaudal and longitudinal subdivisions of the neural tube. However, several recent studies claim to have visualized the early chick neural plate by means of genetic markers at stages 3d-4 (i.e. Rex et al., 1997a; Rex et al., 1997b; Pera et al., 1999; Knoetgen et al., 1999; Darnell et al., 1999; Streit and Stern, 1999); several neural or non-neural ectodermal markers indeed show expression patterns roughly correlative with current ideas on the neural plate. However, it is not yet clear how precisely these expression patterns coincide with experimentally determined fate boundaries.

The experimental analysis of neural specification performed by Darnell et al. (Darnell et al., 1999) showed that the chicken area pellucida rostral to the lengthening primitive line remains unspecified up to stage 3c [stages according to Schoenwolf (Schoenwolf, 1988)]. This led us to elaborate the present fate map in the chick at stages 3d-4, immediately after definitive specification of the neural primordium (Darnell et al., 1999). We eschewed assumptions based on gene expression patterns, interpreting simply graft integration into the wall of the neural tube at stages 9-11. Eventually, the repeated observation that the neural plate was slightly shorter at the rostral midline than expected led us to compare our experimental results with the expression of *Ganf*, a gene reported to label the rostral border of the plate. This pattern was consistent with the experimental mapping data. Some additional gene mapping experiments (probes for *Plato*, *Sox2*, *Otx2* and *Dlx5*) conveyed the need of further research correlating reported neural plate markers with the novel proportions suggested here for the chick neural plate at stages 3d/4.

MATERIALS AND METHODS

Fate-mapping of the neural plate was performed using homospecific, fluorescently labeled, homotopic grafts in New-cultured chick embryos. Fertilized eggs were incubated at 38°C under standard conditions until the embryos reached stages HH3d-4 (Hamburger and Hamilton, 1951). The embryos were explanted upside-down into New culture in agar Petri dishes (New, 1955; Stern and Ireland, 1981), as

described by Schoenwolf and Alvarez (Schoenwolf and Alvarez, 1989). After keeping the cultures for 30 minutes at 38°C, the donor embryos were prepared as follows: a sector of the endoderm was gently stripped away, cutting first along the endophillic crescent, and 1 ml of phosphate buffered saline (PBS) containing 20 μl CFSE stock solution [5(6)-carboxyfluorescein diacetate, succinimidyl ester, or 5(6) CFDA.SE 'mixed isomers'; Molecular Probes C-1157; stock 5 mg/ml in DMSO] and 5 μl rhodamine stock solution [rhodamine 123: xanthylium, 3,6-diamino-9-(2(methoxy-carbonyl)phenylchloride; Molecular Probes R-302; stock 10 mg/ml in DMSO] was applied for 1 hour in the dark. The rhodamine serves to increase the fluorescent signal of the grafts for photographing their position at various times after the operation. In some control cases, quail embryos at an equivalent stage were used as donors.

Grafts

The host embryos were first prepared by separation of the endoderm from the area over the intended graft site. The graft site was precisely localized by means of an ocular grid displaying cartesian and angular coordinates and centered on the node (Fig. 1A) (Fernández-Garre et al., 2002). A glass pipette was then used to punch out a plug of ectoderm in the host embryo (to be discarded), and to obtain an homotopic, isochronic plug in the donor embryo (the pipette mouth bore was callibrated – usually it was 125 μm wide, but a range of 70 to 200 μm was tried out in some cases; Fig. 1B,C). The labeled donor plug, containing approximately 100-300 cells depending on size, was rinsed in saline solution to dilute out excess fluorescent label, and was inserted in the site previously prepared in the host (correct apical versus basal orientation was assessed by the tendency of the basal surface of the ectoderm plug to contract slightly during washing; planar orientation was not conserved). Each graft was recorded photographically at 0 hours (Fig. 1C) and again 24 hours after grafting, just before fixing the embryos in cold 4% paraformaldehyde overnight (by this time they had reached stages 9-11 in most cases; see Tables 1-3).

Some control grafts (n=16) were recorded by time-lapse photography (usually every 30 minutes) for various time periods, or were fixed at various intervals, paraffin-wax embedded and sectioned, to investigate the time needed for full integration and to detect diffusion of label (no diffusion was found). Snugly inserted grafts were well incorporated into the host epiblast by 30 minutes (Fig. 1D). A minority of cases, when the grafts were somewhat loose, needed up to 2 hours for complete incorporation. This quick healing greatly diminishes the possibility of artifacts caused by regeneration effects. No obvious graft deformations or fate differences were observed in these cases, and they were pooled with the rest for interpretation. Fig. 1B illustrates the relative positions and sizes of all the grafts analyzed in this study at 0 hours; an important feature of our approach was that we aimed for substantial saturation of the territory, which aided interpretation later on (see Discussion). Distorted embryos were discarded.

Visualization of the grafts

After fixation, the specimens were washed in cold PBS (2×5 minutes) and passed through increasing concentration steps into cold methanol (25%, 50%, 75%, 100%; 5 minutes each step), in which they were stored at –20°C. The CFSE-labeled cells derived from the graft were identified with anti-fluorescein Fab fragments conjugated either to alkaline phosphatase or to horseradish peroxidase (anti-fluorescein-AP; anti-fluorescein-POD; Boehringer Mannheim, Frankfurt, Germany; use 1:500). The procedure was as follows: embryos were rehydrated stepwise to PBS, washed twice 30 minutes in PBS-T (PBS + 1% Triton-X) and twice 30 minutes in PBS-T-NGS (PBS-T + 4% normal goat serum). Conjugated anti-fluorescein Fab fragments (1:500) were added and the immunoreaction proceeded overnight at 4°C, with gentle agitation. Afterwards, the embryos were washed at least four times for 10 minutes in PBS.

For visualization of alkaline phosphatase-conjugated immunoreactions, we washed first with NTMT solution (2×10 minutes; for 50 ml: 5 ml 1 M Tris + 1 ml 5 M NaCl + 2.5 ml 1 M $MgCl_2$ + 0.5 ml 10% Tween 20 + 41 ml deionized water; 24 mg levamisol were added just before use). The reaction was started by adding 4.5 μl/ml NBT (75 mg/ml in 70% dimethylformamide) and 3.5 μl/ml BCIP (50 mg/ml in 70% dimethylformamide) to the NTMT solution, and was controlled visually. After stopping the reaction in PBT (PBS + 0.1% Tween 20), we usually dehydrated and rehydrated again through the cold methanol series (5 minute steps), a procedure that cleans the background. The specimens were next postfixed in 4% paraformaldehyde overnight, photographed and stored in methanol at –20°C.

For visualization of peroxidase-conjugated immunoreactions, diaminobenzidine tetrahydrochloride (DAB) was employed, using Sigma Fast 3,3′-DAB tablets diluted according to manufacturer instructions (Sigma, Alcobendas, Madrid). The reaction was stopped in PBS, and the embryos were postfixed, photographed and stored. Quail grafts were visualized by means of the QCPN antiquail monoclonal antibody (Developmental Hybrydoma Bank, Iowa).

Sectioning

Specimens were first brought to PBS, dehydrated through a buthanol series (30%, 50%, 70%, 96%, 100%; 5 minute steps) and then embedded in paraffin wax, passing through buthanol/paraffin wax mix 1:1 (10 minutes) and several changes of pure paraffin wax (1 hour each). Transversal sections were obtained at a thickness setting of 10 μm, deparaffinized in xylene and mounted with Eukitt.

In situ hybridization

Several specimens with homotopic grafts were processed for detection of *Ganf* gene expression (cDNA provided by M. Kessel, Göttingen). The cDNA was linearized with *Hin*dIII, obtaining an antisense mRNA probe that was labeled with digoxigenin and used for whole-mount in situ hybridization according to Shimamura et al. (Shimamura et al., 1994). Additional unoperated specimens were processed similarly with antisense chicken mRNA probes for the genes *Ganf* (M. Kessel, Göttingen), *Plato* (G. Schoenwolf, Salt Lake City), *Sox2* (P. J. Scotting, Nottingham), *Otx2* (A. Simeone, London) and *Dlx5* (J. L. R. Rubenstein, San Francisco). Some control grafts were photographed just after the operation, and again after fixation and after in situ hybridization with various probes, checking for eventual retraction of the tissue during processing (no retraction after fixation; 3% retraction after in situ).

RESULTS

The fate-mapping data obtained are summarized in Tables 1-3 and will be described in the following five sections, addressing (successively) the neural plate border at stages 3d-4, the rostral midline, the major anteroposterior neural territories, prospective dorsoventral longitudinal regions and the correlation of fate map results with gene expression data.

The border of the neural plate at stage 4

Fig. 1B shows the positions and sizes of all the grafts analyzed in this study (at 0 hours post-operation). In our records (Tables 1-3), each graft 'site' was identified by case number, angular position relative to the median axis of symmetry centered in the node (angle α in Fig. 1A) and the distances to the node edge (broken line in Fig. 1A) of the proximal and distal edges of the graft. Snugly inserted grafts were fully incorporated after 30 minutes, irrespective of their location (Fig. 1C,D).

Fig. 2 illustrates three representative cases at different

Table 1. Cases ordered by topography and fate (non-neural fates)

Case number	α	Distance from node (μm)	∅ (μm)	Stadium		Non-neural ectoderm (at level of)				Mesoderm		Endoderm
				Oper	Fix.	Pros.	Mes.	Rhomb.	Spin.	Somitic	Lateral	
Non-neural fates												
L-55	0	270-395	125	3d	10	XXX						
L-125b	0	280-405	125	4	9	XXX						
P-22	0	280-450	170	3d	9–	XXX						
P-21	0	400-560	160	3d	9+	XXX						
P-35	0	400-570	170	4+	9+	XXX						
L-67	0	280-405	125	4	10	XXX	XXX					
L-75b	0	280-405	125	4	11+	XXX	XXX					
P-29	15	400-600	200	4	10+	XXX	XXX					
P-37	15	380-550	170	3d	10	XXX						
L-33	20	375-500	125	4	10	XXX	X					
L-4b	25	415-540	125	4	9	XX	XX					
P-6	30	440-610	170	4	9+	XXX	XXX					
P-8	35	480-650	170	4	9	XX	XXX					
P-12	35	700-800	100	4	7	XX	XXX					
P-20	40	450-580	130	3d	9	XX	XXX					
L-105b	45	460-585	125	3d	10+	XX	XXX					
L-70b	45	480-605	125	4	13+	XX	XXX					
P-16	45	560-730	170	4	8	XX	XXX					
P-9	50	450-620	170	4	11+	XX	XXX					
L-84	50	460-585	125	3d	10	XX	XX					
L-103b	55	400-525	125	4	12		X	XXX				
P-17	60	565-835	270	3d	8		X	XXX				
P-18	65	400-670	270	3d	10		X	XXX				
P-19	65	430-600	170	3d	9		X	XXX				
L-85b	65	360-485	125	4	11			XXX				
P-41	75	325-450	125	3c	11–			XXX				
P-36	75	450-620	170	4	9			XXX				
L-68b	75	320-445	125	4	13+			XX				
L-85	80	325-450	125	4	11			XX				
P-40	80	400-525	125	4	10			XX	X			
P-42	85	275-415	140	3d	9			XX	X			
L-149b	110	200-325	125	3d	9					XXX	X	
P-46	110	190-330	140	4	10						XX	
L-106	125	90-215	125	4	11+					XXX		
L-97b	125	175-300	125	4	11+					XXX		
L-96b	130	175-300	125	4	10–					XXX		
L-148b	130	250-375	125	4	9+						X	
L-78	135	45-170	125	4	10					XXX		
L-8b	135	50-175	125	4	9					XXX		XX
L-86-2	135	80-205	125	4	10					XXX		
L-76b	145	60-185	125	4	13					XXX		
L-99b	150	60-185	125	4	11						XXX	
L-44	150	75-200	125	4	10						XXX	

X, few cells; XX, partial; XXX, large; XXXX, massive.

angular positions, in which the grafts contributed exclusively to non-neural ectoderm. All the CFSE-labeled cells derived from these grafts lay outside the closing neural tube (arrowheads in Fig. 2B,D,F). Fig. 4B shows in green the positions and sizes of all grafts producing such extraneural epiblastic labeling (the caudalmost ones labeled prospective mesodermal and endodermal tissues; see Fig. 6D,E).

Grafts placed slightly more concentrically clearly fell across the border of the neural plate, producing derivatives both outside and inside the closing neural tube, eventually also in the neural crest or the otic placode. Fig. 3A shows the topography of all such mixed cases at time 0 hours, and Fig. 3B-G illustrates some representative results, highlighted in green in Fig. 3A. The midline cases show labeled cells in the ventral head epiblast as well as in the rostral forebrain (arrowheads; Fig. 3B-D). The lateral cases show neural label at the roof of the neural tube and associated extraneural label in the neural crest and nearby surface ectoderm (Fig. 3E-G). The neural cell patches were usually rather compact, though occasionally some graft-derived cells appeared isolated at some distance, or even in the contralateral neural ridge, at points where the neural canal was not closed (not shown); this last surprising aspect suggests that the unfused neural ridges may establish transient contacts that allow some graft-derived cells to jump contralaterally.

Our rationale for approximating the boundary of the neural plate is presented graphically in Fig. 4A-C. First, we superposed graphically the set of all grafts labeling any extra-neural areas (in Fig. 4A, blue) upon the set of grafts labeling any neural tube (in Fig. 4A, orange). Grafts at the intersection of these sets appear dark green in color. They are those that contribute various amounts of neural and non-neural ectoderm. The neural/non-neural boundary must lie somewhere inside this intersection, though some parts of it are less precisely

Table 2. Cases ordered by topography and fate (plate boundary and alar fates)

Case number	α	Distance from node (μm)	∅ (μm)	Stadium		Neural ectoderm (at level of)				Mesoderm		
				Oper	Fix.	Pros.	Mes.	Rhomb.	Spin.	Somitic	NNE	Endoderm
Neural plate boundary												
L-25	0	105-275	170	4	10	XXXX					X	
L-30	0	150-275	125	4	9	XXXX					XX	
L-141b	0	180-305	125	4	9+	XXXX					XX	
L-28	0	200-325	125	4	10–	XXXX					XX	
L-34	0	240-365	125	4	9+	X					XX	
P-26	0	240-410	170	3d	10+	X					XX	
L-113b	10	175-300	125	4	11	XXe					X	
L-146b	10	225-350	125	4	9+	X					XX	
P-3	15	250-420	170	4	8	X					XX	
L-80	20	315-485	170	4	9	X					XX	
L-74b	30	450-575	125	4	13	X	X				XX	
P-7	40	380-505	125	4	10		XXXX				X	
L-77	65	190-315	125	4	9+			XXXX	X		X	
L-109	70	270-345	75	3d	10			XXX			XX	
L-89b	90	195-270	75	4	10				XXXX		X	
L-102b	95	190-315	125	4	11				XX	XX	XX	
L-7b	115	0-125	125	4	9				XX	XXX		
L-110	125	0-125	125	4	10				XX	XXX		
L-134b	130	25-150	125	4	9				XX	XXX		
L-56	130	0-90	90	4	9+				X	XXXf		X
Alar plate												
L-137b	0	125-200	75	4	9	XXXX						
L-77b	15	150-275	125	4	11+	XXe						
L-115b	25	90-190	100	4	12	XXe						
L-82	30	175-300	125	4	8	XXe	XX					
P-5	35	175-345	170	4	10+	XXe	XX					
P-39	40	250-375	125	4+	10+	X	XXX					
L-131b	40	325-450	125	5	11	X	XXX					
L-86-1	40	335-460	125	4	10		XXXX					
L-114b	45	300-375	75	4	11	X	X					
P-13	50	280-405	125	4	10–		XXXX					
L-113	70	170-295	125	4	8		X	XXXX				

X, few cells; XX, partial; XXX, large; XXXX, massive; e, eye vesicle labeled; f, floor-plate labeled.

approximated than others, owing to the differences in the diameters of the grafts; also note some gaps exist where we lack data (white areas). Our next step was to map separately in Fig. 4B all the cases whose derivatives were entirely within the neural tube (yellow) from those whose derivatives are wholly extra-neural (green). The excluded intersectional cases are still represented (transparent), thus allowing visualization of their relative sizes and positions (Fig. 4B). One specific intersectional case clearly labeled the otic placode (thicker outline in Fig. 4B; see Fig. 3F).

On the whole, the 'neural' and 'non-neural' sets of grafts in Fig. 4B are separated by a gap partially thinner than the previous intersectional territory in Fig. 4A, and the neural plate boundary (where prospective neural and non-neural cells may interdigitate or not) must lie inside this border gap. Fortunately, some cases among these three sets (coded transparent, green or yellow in Fig. 4C) minimally differed in position with other neighboring cases, or overlapped mutually only slightly inside the 'border gap'; some 'yellow' grafts practically touched 'green' ones across the gap. Three border cases (L34, L30 and L146b) at, or close to, the rostral midline defined a thin overlap zone, 35 μm wide (Fig. 4C). Our rationale here is that, as all three cases cross the border, having distinct neural and non-neural derivatives at the stage examined, the boundary zone must be smaller than their joint graphic intersection – otherwise they would not be border cases – and therefore must lie within this 35 μm wide zone. The bisecting border line drawn by us therefore assumes a possible error in estimating the actual width and position of the border zone smaller than 17.5 μm. In addition, one case at the rostrolateral angle of the plate had only a very small neural component, and three small grafts placed along the apparent border in the caudal half of the neural plate corroborated the position of the boundary (Fig. 4C; compare Fig. 3G). Following the practice of all previous neural plate fate maps, our neural plate border was extrapolated between these points (Fig. 4C; Table 2). A line boundary is useful for practical application of the fate map, but we should emphasize that the boundary might be conceived (defined) as a band of epiblast, the thickness of which changes with time (see Discussion). In any case, our data clearly suggest that at stage 4 such a band probably would be thinner than the border gap in Fig. 4B. Relevant measurements relating the hypothetical linear border to the periphery of the node and to the caudal prospective mesodermal area appear in Fig. 6E.

The rostral midline

A constant feature of our experiments refers to their laterality. All grafts placed across the median radium (directly rostral to the node) later produced nearly symmetrical derivatives on both sides of the forebrain and/or median non-neural ectoderm

Table 3. Cases ordered by topography and fate (alar/basal and basal fates)

Case number	α	Distance from Hensen's node (μm)	∅ (μm)	Stadium		Neural ectoderm (at level of)				Mesoderm	Endoderm
				Oper	Fix.	Pros.	Mes.	Rhomb.	Spin.	Somitic	
Alar-basaltransition											
L-68	0	75-200	125	4	9+	XXXXe					
P-4	35	70-240	170	4	10–	XXe	XX				
L-108	50	125-250	125	3d	8		XXXX				
L-84b	50	170-295	125	3d	10	X	XXXX	X			
L-94b	75	125-250	125	4	10			XXXX	X		
L-101b	80	125-250	125	4	12			XX	XXX		
L-71b	95	75-200	125	4	12				XXXX		
Basal plate											
L-140b	0	0-125	125	4	8	XXX					X
L-145b	0	0-125	125	4	9–	XXXX				X	
L-36	0	0-125	125	4	10	XX					
L-27	0	0-125	125	4	9	XXX					
L-117b	15	0-125	125	4	10+	XX	X				
L-82b	20	0-125	125	4	13+	XX	XX				
L-26	30	0-125	125	4	9	XX	XX				
L-116b	40	75-200	125	4	9	XX	XXXX				
L-135b	40	0-100	100	3d	9	X	XXXX				XX
L-79	45	0-170	170	4	10	X	XXXX	X			X
L-35	45	0-125	125	4	10	X	XXXX	X			
L-118b	60	0-70	70	3d	9–		XXXX	XXXXf			
P-2	70	125-261	136	3d	10			XX	XX		
P-31	80	25-175	150	4	10+			XXXX	XXX		
P-1	80	35-175	140	3d	9			XXX	XXX		
L-76	90	0-140	140	4	10			XXX	XXX		
L-81b	90	0-125	125	4	13				XX		
L-38	90	25-150	125	3d	9			XX	XX		
L-86b	90	90-170	80	3d	11				XXX		
L-111	100	0-125	125	4	11+				XXX		
L-107	100	40-165	125	3d	9+				XXX		

X, few cells; XX, partial; XXX, large; XXXX, massive; e, eye vesicle labeled; f, floor-plate labeled.

(see Figs 3, 8, 10). These symmetric median domains did not extend into the laterally placed optic vesicles. All grafts positioned wholly outside of this median area had a corresponding unilaterally labeled domain (e.g. the massive 'eye' case shown in Fig. 5B,G,H). Within the limits of resolution allowed by the size of our grafts, there was thus no evidence of cell intercalation across the forebrain midline after stage 4. We accordingly introduced a forebrain midline boundary in our schemas (e.g. Fig. 4, Fig. 6D).

Prospective major anteroposterior territories

The different grafts giving rise to neural derivatives were also rated as regards the rostrocaudal topography of their derivatives in the neural tube at stages 9-11 (Tables 2, 3; Fig. 5A). This interpretation rested on the characteristic morphology of some brain parts (i.e. forebrain with optic vesicles; sphericity of mesencephalic vesicle; isthmic constriction; thin spinal cord lumen), and on several extraneural landmarks (otic placodes, notocord, heart, pharynx, anterior intestinal portal, branchial arches, somites).

Fig. 5A-F illustrates five examples of grafts mapped as wholemounts 24 hours after the graft, indicating in each case the recorded location of the graft (corner insets). One graft squarely labeled the eye vesicle (Fig. 5B,G,H). More caudal positions labeled diencephalon and midbrain (Fig. 5C,D,I-L). Note that labeling of lower brainstem and spinal cord coincided with postnodal grafting loci (Fig. 5E,F,M-P). Fig. 6A joins all the data analyzed as regards rostrocaudal fate (see also Tables 2, 3); we color-coded the sets of grafts judged to lie mainly in the forebrain, midbrain, hindbrain or spinal cord, thus emphasizing the overlaps found between these sets. We estimated that the tentative boundaries between these prospective brain regions can be approximated for practical uses by the black lines bisecting these overlap areas (see Discussion). All the regions analyzed are wedge-shaped and expand peripherally (Fig. 6A,D). Table 4 gives the rough length of each brain subdivision as measured either close to the node (paranodal length) or to the peripheral border of the neural plate (peripheral length). The postulated prospective transverse boundaries were slightly bent in a rostralward direction and lay at ~40°, 60° and 80° with regard to the midline (Fig. 6D). The end of the spinal cord anlage lies at ~120° radius.

Fig. 6B in addition shows the prospective optic vesicle area, which can be mapped thanks to its incipient evagination at stages 9-11; this primordium appeared either labeled or unlabeled in a number of cases (n=13). Its central location was identified by case L-82 cited above (Fig. 5B,G,H). Fig. 6B compares in detail seven yellow-coded grafts (including L-82)

Table 4. Length of anteroposterior regions (HH4)

	Paranodal (μm)	Peripheral (μm)
Forebrain	73	350
Midbrain	57	190
Hindbrain	53	200
Spinal cord	60	180

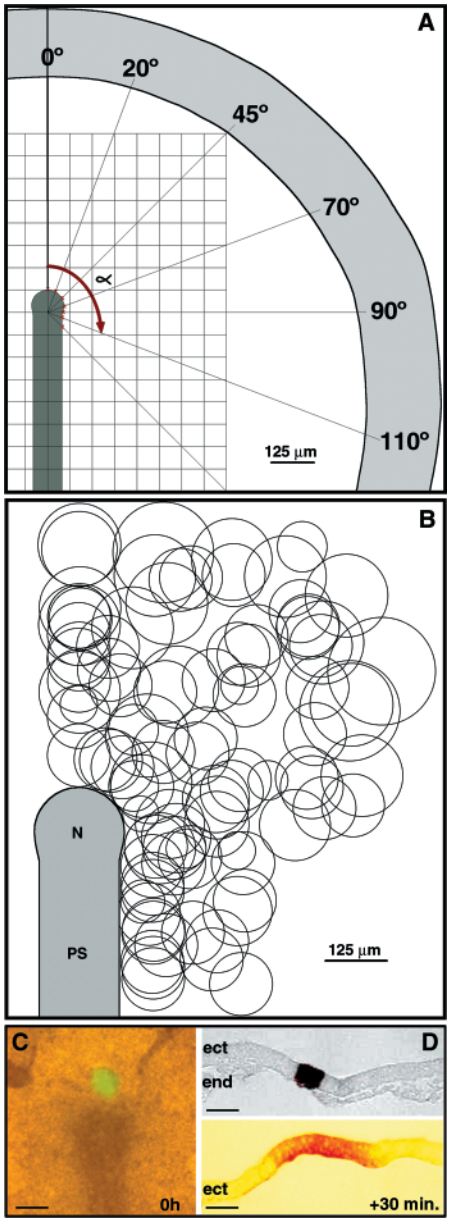

Fig. 1. Experimental design used in the present fate map. The epiblast at full-length primitive streak stage (stages 3d/4) was visualized through a grid centered upon the node (A) and plugs of labeled donor tissue were transplanted (circles in B; normally 125 μm in diameter; range 70-200 μm) at different radial locations (α in A). Positions of labeled grafts was recorded by fluorescence microscopy just after transplantation (C) and also after 24 hours survival. Control cases fixed and sectioned at 30 minute intervals revealed that most grafts appeared well integrated within 30 minutes (a small and a larger case are shown sectioned frontally in D), though occasionally some needed up to 2-2.5 hours for complete integration. For a more precise description see text. N, Hensen's node; PS, primitive streak. Scale bars: 100 μm in C,D.

contributing selectively to different parts of the optic vesicle. Six additional grafts labeled diverse forebrain/midbrain areas, but stopped just outside the optic evagination; they are shaded in light blue in Fig. 6B (resulting green overlap zones are understood as falling outside the eye field). The optic

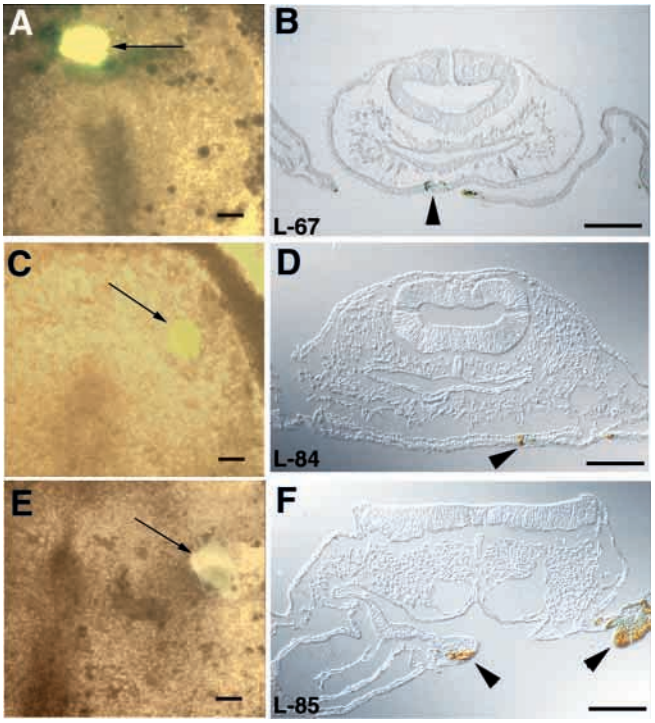

Fig. 2. Three representative cases in which CFSE labeled grafts (thin arrows in A,C,E) contributed to non-neural ectoderm.
(A,C,E) Fluorescence images at 0 hours (graft position relative to the node); (B,D,F) corresponding immunolabeled transverse sections of the same embryos fixed after 24 hours. Cells derived from the graft can be identified in non-neural ectoderm by the DAB label (arrowhead). Scale bars: 100 μm in B-G.

primordium was thus mapped tentatively according to these data between the 20° and 40° radial lines. Note these data do not distinguish prospective neural retina versus pigmented retina and optic stalk areas.

We could not identify either the telencephalon or the olfactory placode, as they remain morphologically indistinct within the survival time employed. However, the rostrolateral forebrain grafts peripheral to the optic field must have contained the prospective telencephalon (Couly and Le Douarin, 1985; Couly and Le Douarin, 1987; Rubenstein et al., 1998; Cobos et al., 2001). Note the extreme rostral position of the dorsal midbrain primordium in Fig. 6A, which is supported specifically by data from grafts such as P-7 (40° line; 380-505 μm; Fig. 3E, Fig. 7C), case L-131bis (40° line; 325-450 μm; Fig. 7D) and case L-74b (30° line; 450-575 μm; see Table 2). One of our cases clearly labeled the dorsal part of the otic placode; this was a small mixed graft at the periphery of the prospective hindbrain (L-109; Fig. 3A,F; thicker outline in Fig. 4B). Some of the non-neural grafts in this area (see Fig. 4B) either labeled the entire placode inside a large grafted epiblast domain, or approached it ventrally, without distinct labeling inside it. This suggests that the anlage may be rather small at stage 4, but our data are insufficient to postulate a border for it.

Prospective dorsoventral longitudinal regions

Dorsoventral patterning of the early neural plate and tube can be roughly modeled by the classical four longitudinal regions

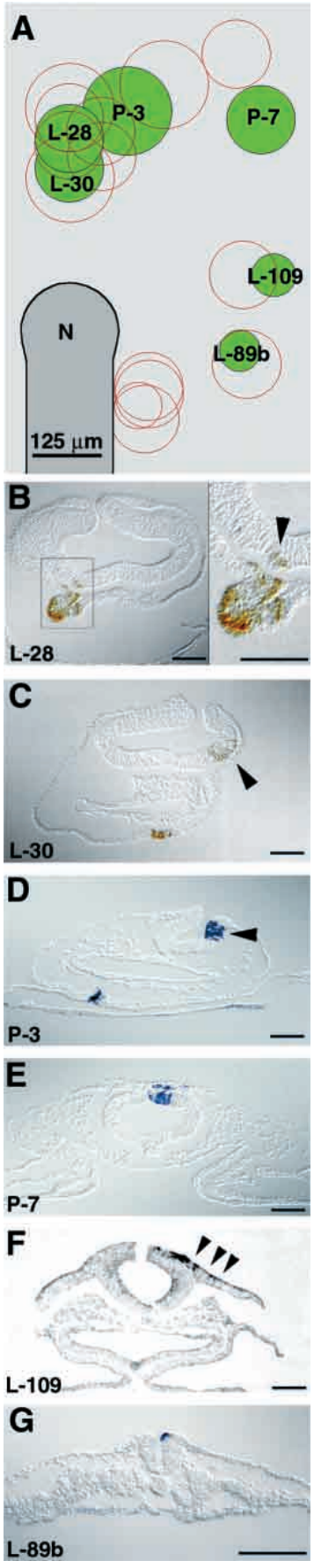

Fig. 3. Examples of cases in which the grafted tissue contributed to both neural (arrowheads in B-D; unmarked in E-G) and non-neural ectoderm. The variously overlapping grafts that overstepped the neural border are represented in A. Cases illustrated in B-G are tagged and green in A; cross-sections in B-G show the locations of the transplanted cells, stained either with DAB (brown) or with AP (blue). Arrowheads in F show label in the otic placode; adjacent sections also had label in the dorsal neural tube. Scale bar: 100 μm.

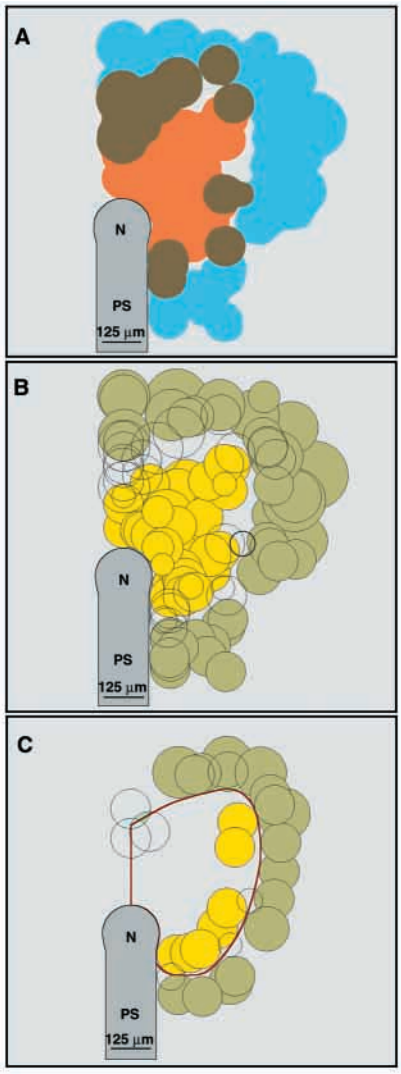

Fig. 4. (A) The overlap (brown) between the grafts labeling inclusively some neuroectoderm (orange), versus those labeling some non neural ectoderm (blue). Grey areas represent loci not sampled with grafts. (B) Topography and relative size of all studied cases at 0 hours, color-coded according to neural versus non-neural fate. Green identifies the grafts contributing exclusively to non-neural ectoderm and yellow corresponds to grafts producing exclusively neural ectoderm. The separating gap should contain the neural plate boundary, but is probably larger than the border itself. The border grafts contributing to both neural and non-neural regions are represented as empty circles (compare with this set isolated in Fig. 3A). The small empty circle highlighted by a darker outline represents the single case that selectively labeled the otic placode (compare with Fig. 3F). (C) Selection of cases which collectively allowed a more precise definition of the neural border (red line), with some extrapolation (see Results). N, Hensen's node; PS, primitive streak.

of His (roof, alar, basal and floor plates), as there is evidence for their widespread existence in vertebrates as precocious molecularly specified territories (Puelles and Rubenstein, 1993; Shimamura et al., 1995; Shimamura et al., 1997; Hauptmann and Gerster, 2000). For our analysis of dorsoventral prospective topography, we assumed on the basis of available data (e.g. *Shh* versus *Pax6* or *Dlx* gene expression

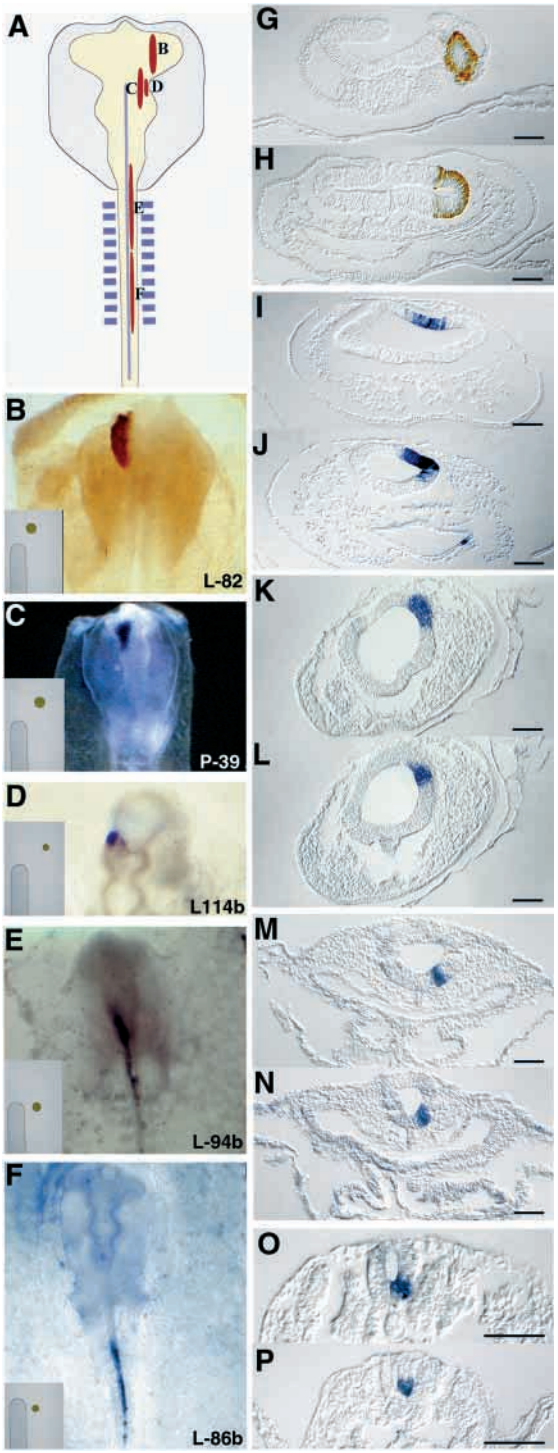

Fig. 5. (A-F) Schematic (A) and microphotographic examples (B-F) of whole-mount DAB or AP labeled graft derivatives obtained 24 hours post-operatively, illustrating different positions mapped along the anteroposterior dimension of the neural tube (insets in B-F show the positions of the five grafts at 0 hours). The relative position of the labeled cells at stage 10 is shown in A. Note that the circular grafts at stage 4 adopt an elongated configuration because of cell rearrangement along the neural axis (red areas in A) (Schoenwolf and Alvarez, 1989). Representative sections of these whole-mounts are presented in the right-hand column. (G,H) Optic vesicle (from B); (I,J) caudal forebrain and alar mesencephalon (from C). (K,L) rostral midbrain (from D); (M,N) caudal mesencephalon and rhombencephalon (from E); (O,P) spinal cord (from F). Scale bar: 100 μm.

domains in the forebrain) that the chick alar plate at stages 9-11 may roughly correspond to the dorsal two thirds of the lateral wall of the neural tube (even more where it includes the budding optic vesicles, which are assumed to be alar), whereas the basal plate roughly represents the remaining ventral third. The floor plate is much thinner, and usually is histologically distinct at the ventral midline. Our results were not discriminative enough to resolve the prospective roof plate from the alar plate or the neural crest.

Fig. 6C and Fig. 7A map all grafts (at 0 hours survival) estimated to contribute at least in part to the prospective alar plate, defined as stated above (see also Table 2). Some representative examples are illustrated in Fig. 7B-E. Other cases mentioned above also showed data for grafts giving rise to alar domains (see Fig. 3; Fig. 5B-D,G-L). Similarly, Fig. 6C and Fig. 8A map all grafts (0 hours survival) estimated to contribute at least in part to the prospective basal plate and floor plate (see Table 3). There also appeared to be a substantial overlap between the sets of all grafts thought to label the majority of either the alar plate or the basal plate (brown domain in Fig. 6C). We traced our tentative prospective alar/basal limit as a sigmoid line bisecting this overlap area, also applying an assumption that alar plate domains should primarily be continuous with prospective non-neural ectoderm, whereas basal/floor domains should be topologically continuous with prospective intra-embryonic mesoderm/endoderm (Fig. 6C,D; Table 3; see Discussion).

Only a few of our cases extended into the floor plate at hindbrain or spinal cord levels. The cases L-118b and L-56 distinctly labeled floor plate tissue, in addition to adjacent basal plate (Fig. 8J-L; Table 3). Comparison of the relative topography of these cases suggested that they were placed some 15-20 μm closer to the primitive line than others at the same rostrocaudal level, which labeled exclusively basal plate. However, other cases recorded as placed at the same nominal distance only labeled basal plate (compare Fig. 1B; Table 3), suggesting that the dimension of the floor plate domain may be barely within the resolution power of our experimental approach. Our representation of the prospective floor plate in Fig. 6D is therefore more tentative than that of the basal plate.

Graft location at the forebrain midline correlated with *Ganf* expression

Expression of *Ganf* mRNA first appears at stage 4 in the rostral forebrain, including the rostral neural plate boundary (Fig. 9A) (Knoetgen et al., 1999). Later it consistently identifies the apparent border of the rostral neural plate [Fig. 2E-G,L by Knoetgen et al. (Knoetgen et al., 1999) (our whole-mount data at stages 5-10; not shown). At stages 9-11 we mapped *Ganf* in experimental embryos that received homotopic CFSE-labeled grafts of forebrain midline tissue at diverse distances from the nodal perimeter, in order to corroborate the estimated location of the rostral neuropore at the midline. Grafts placed close to the node fell well behind the *Ganf* domain (Fig. 9B-D). Grafts traversing the edge (n=2) [i.e. case L-146bis, 10° line; 225-350

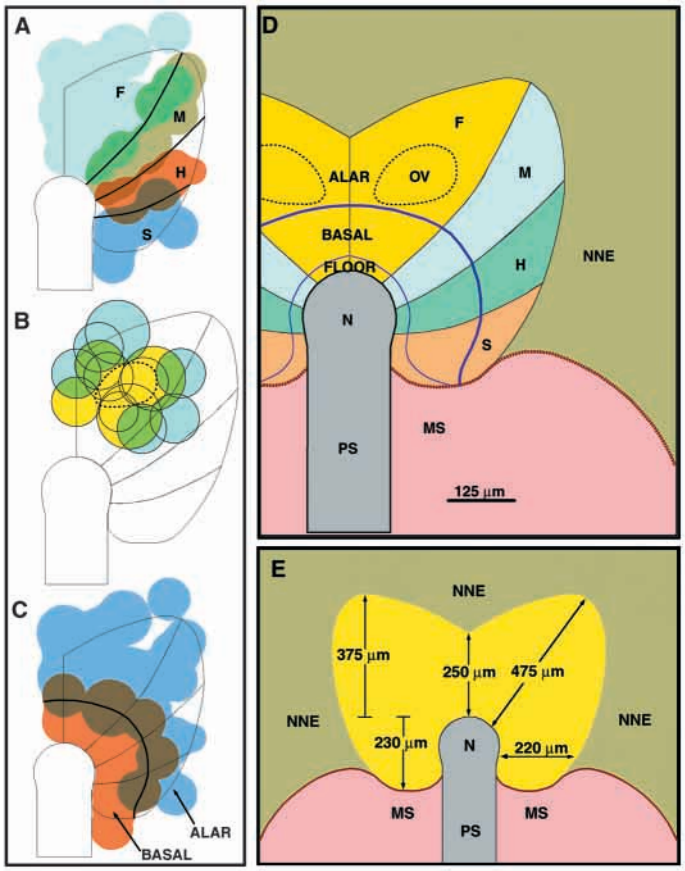

Fig. 6. (A) Graphic representation of the sets of grafts classified according to their main rostrocaudal derivatives. The arbitrary color code allows visualization of the areas of overlap between these sets (color summation), and thus tracing of the estimated prospective transverse boundaries (see Discussion). (B) Set of grafts found useful for characterizing the eye field (broken outline); six grafts shown in light blue ended just outside the eye vesicles, whereas seven yellow-colored grafts labeled partially the eye vesicle (see also Table 2). (C) Graphic superposition of color coded sets of grafts labeling the alar and basal plate regions; the overlap between these sets is highlighted by color summation (brown), roughly indicating where to trace the postulated longitudinal alar-basal boundary (thick black line). (D) Detailed fate map obtained, showing the longitudinal and transverse boundaries identified within the prospective neural territories at stages 3d/4. The floor plate territory was marked as well (see Results and Discussion). (E) The estimated main radial, longitudinal and transversal distances relative to the node are indicated for the stage 3d/4 neural plate fate map (yellow). F, forebrain; M, midbrain; H, hindbrain; S, spinal cord; MS, mesoderm; NNE, non-neural ectoderm; PS, primitive streak; OV, optic vesicle.

μm (just 25 μm inside the estimated midrostral boundary)] produced only a handful of grafted cells at the rostral edge of the neural plate, overlapping with *Ganf* expression (arrowhead in Fig. 9E,F); other graft-derived cells fell outside the rostral neuropore (Fig. 9F,G). All these results therefore were consistent with our previous estimate of 250 μm as the prenodal length of the neural plate midline.

Other gene expression patterns

We analyzed the expression patterns at stages 3d-4 of four additional genes, *Plato*, *Sox2*, *Otx2* and *Dlx5*, to assess their expression topography relative to the neural plate fate map. *Plato* was reported as a marker of the node and anterior neural tissue (Lawson et al., 2000). Its expression was scarcely visible at stage 3d, but a distinct signal appeared in the rostral neural plate at stage 4. The expression at the midline was roughly co-extensive with the mapped rostral median neural plate and its border, but transcripts were not clearly detectable laterally in the neural plate (Fig. 10A). The expression of *Plato* covers only the medial aspect of the eye fields (Fig. 10A).

Sox2 expression is thought to be neural plate specific (Rex et al., 1997a). Our data corroborated this, because at stage 4 there was strong transcription at the circumnodal (basal plate) area mapped (ending at 200-250 μm postnodally), while peripheral alar areas had weaker signal levels. Weak expression seemed to extend somewhat into nearby non-neural ectoderm and mesoderm areas (Fig. 10B).

Otx2 was reported to be expressed in most of the neural plate area during gastrulation, later becoming restricted to areas rostral to the isthmus (Bally-Cuif et al., 1995). In our material, the territory expressing *Otx2* at stages 3d/4 overlapped the whole mapped neural plate area, but also clearly extended beyond it into neighboring non-neural ectoderm, particularly rostrally, laterally and caudally (Fig. 10C). The *Otx2* signal seems stronger in prospective alar and roof neural areas, being

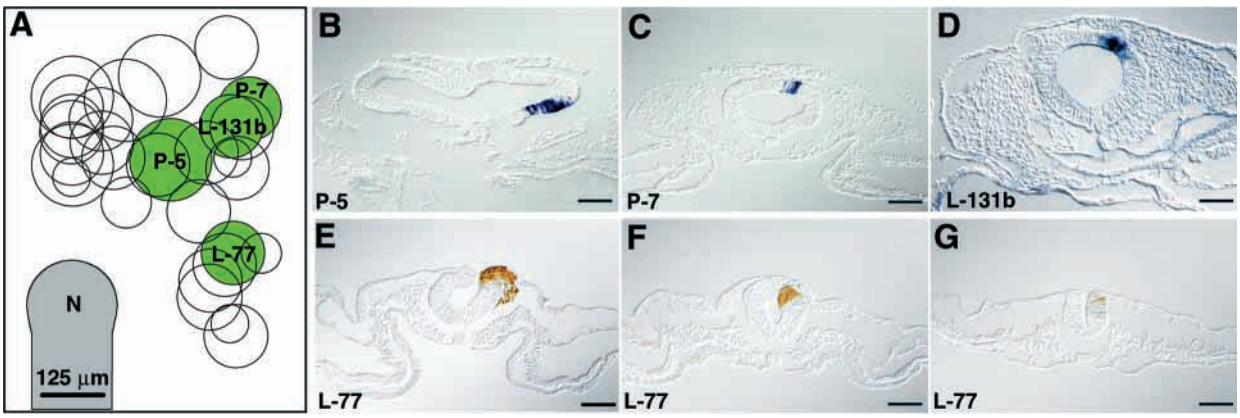

Fig. 7. (A) Set of grafts that contributed to the alar plate. Tagged green circles in the drawing identify the representative examples of which cross-sections are presented in B-G. (B) underside of eye vesicle; (C,D) dorsal midbrain; (E-G) hindbrain. Scale bar: 100 μm.

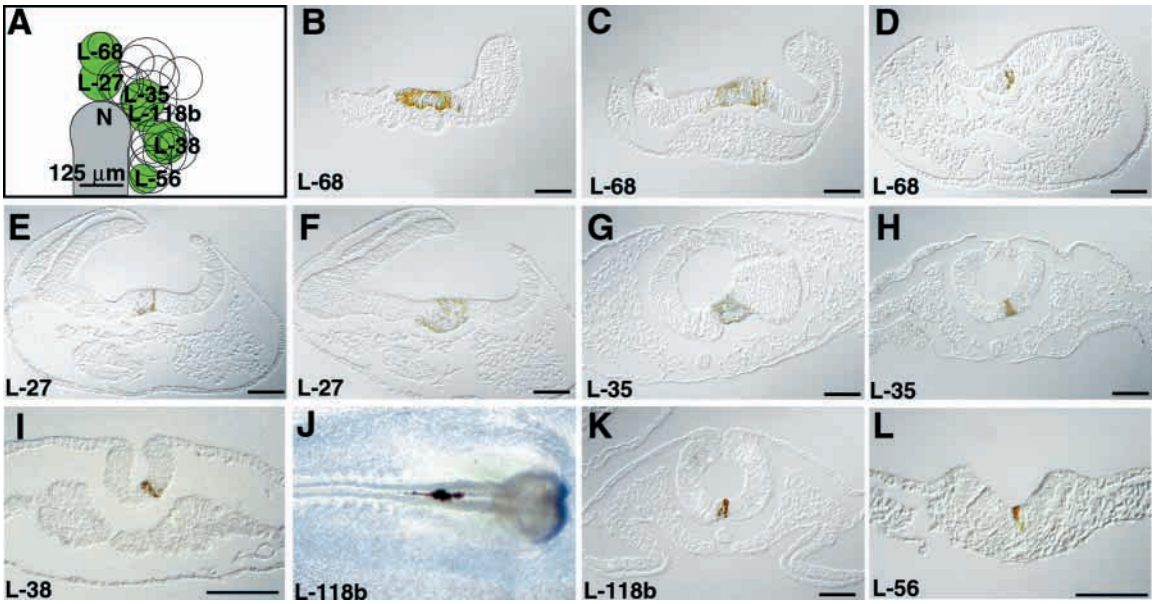

Fig. 8. (A) Grafts that contributed to the basal plate and/or floor plate. Tagged green circles identify the representative examples whose cross-sections are presented in B-L. (B-D) Graft overlapping alar chiasmatic region and basal hypothalamus, (E,F) hypothalamic basal plate and floor; (G,H) midbrain floor and basal plate; (I) basal hindbrain; (J,K) whole-mount view and section of hindbrain floor plate; (L) spinal cord floor plate. N, Hensen's node. Scale bars: 100 μm in B-G.

distinctly weaker in prospective basal neural areas (opposite to *Sox2*); the *Otx2* domain becomes very weak caudal to the neural/mesoderm boundary.

Dlx5 was described as a marker of prospective non-neural epithelium (Pera et al., 1999). Strong expression at stage 4 appeared in a band that was clearly somewhat removed from the neural plate border (particularly caudally), the rostral part of this band seemed to be nearly parallel to the peripheral boundary of Otx2 signal in the non-neural ectoderm (Fig. 10C,D). The Otx2 and Dlx5 limits are approximately tangential to the prominent prospective midbrain roof at the 40° angular position (at 475 μm from the node; Fig. 6D,E; Fig. 10C,D).

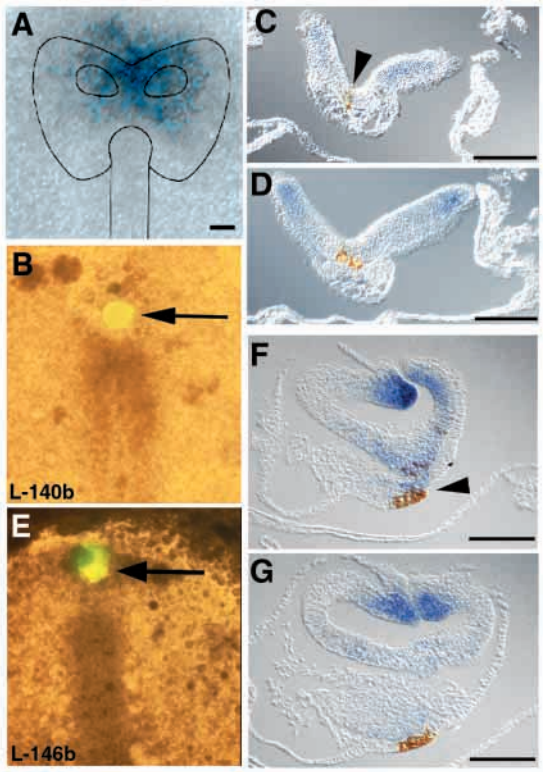

DISCUSSION

This map projects the topology of the initial stage of neural plate differentiation (Darnell et al., 1999) upon the closing neural tube when it is still largely undifferentiated. Earliest neuronal differentiation in the chick forebrain was recorded at stages 11-12 (Puelles et al., 1987). In the following sections we comment on the methodology followed, the limits of the neural plate, rostrocaudal and longitudinal divisions, the eye field and correlations with gene expression patterns.

Fig. 9. Examples of experiments aimed to evaluate the relative final position of grafts made rostral to the node with respect to the anterior neural marker gene *Ganf*. (A) Initial *Ganf* expression pattern at stage 4. (B-D) Embryo transplanted just rostral to the node (0-125 μm) and allowed to develop until stage 8. There is no overlap between the grafted cells in the prospective hypothalamic floor (brown DAB reaction product; arrowhead in C) and the expression domain of *Ganf* (blue signal). (E-G) Embryo with a median graft located between 225-350 μm and allowed to develop until stage 9+. Most cells of the graft (in brown) appeared in the rostral head ectoderm (non-neural tissue), but the anterior region of *Ganf* expression (blue) at the neuropore in F shared some cells with the graft. Therefore, the anterior limit of the established fate map coincides with early and later *Ganf* expression at the neural canal boundary. Scale bars: 100 μm in B-L.

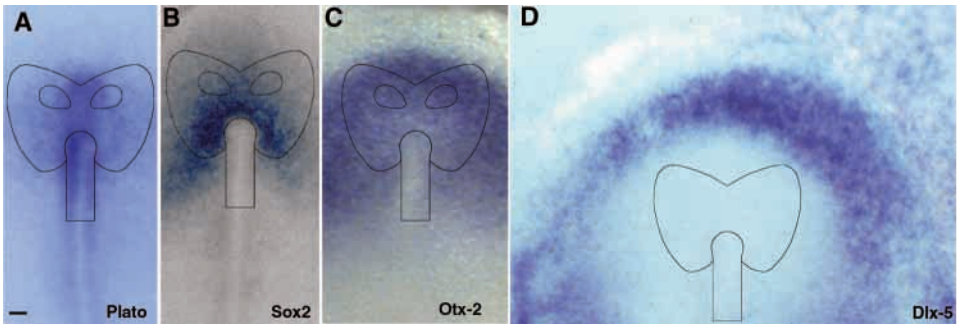

Fig. 10. Whole-mount in situ hybridization reactions to show the expression of the genes *Plato* (A), *Sox2* (B), *Otx2* (C) and *Dlx5* (D) at stage 4 and their relationship with the fate-mapped neural plate boundary obtained in the present study, after correcting for 3% retraction caused by the method used (neural plate outlined in each case). Scale bar: 100 μm.

Methodology

To optimize the reliability of the fate map, we sampled the relevant epiblast area nearly to saturation with multiple overlapping and well-localized plug grafts (previous studies using similar grafts were based upon non-overlapping experiments at fewer sites). The results were visualized with sensitive Fab-fragment immunocytochemical detection of the fixed intracellular CFSE marker (see Darnell et al., 2000). Control cases sectioned or photographed at various intervals did not reveal appreciable diffusion of label from the grafts (Fig. 1D). Operating pipettes with given bore diameters were repeatedly used in successive experiments, thus standardizing the size of the host reception sites and the transplanted cell plugs. One disadvantage of this method is that the planar AP and ML orientation of the graft is lost during the washings and pipetting. However, the overall consistency of our results and previous data using this approach (e.g. Alvarez and Schoenwolf, 1991; Schoenwolf, 1991; García-Martínez et al., 1993; Lopez-Sanchez et al., 2001) suggest that the grafts behave according to their relative position in the host. The grafts integrated in the host in 30-120 minutes. This is less than the length of one cell cycle (Smith and Schoenwolf, 1987), so that artifacts due to tissue regeneration can be largely discounted.

The limit of the neural plate: comparison with previous mappings

As regards the overall shape and extent of the neural plate at stages HH3d-4, our results can be compared with several earlier contributions (Wetzel, 1936; Rudnick, 1944; Spratt, 1952; Rosenquist, 1966), as well as with more recent work (Nicolet, 1970; Nicolet, 1971; Vakaet, 1984; Schoenwolf and Sheard, 1990; Alvarez and Schoenwolf, 1991; Schoenwolf, 1992; Bortier and Vakaet, 1992; García-Martínez et al., 1993; Lopez-Sanchez et al., 2001).

An overview of the sets of grafts labeling either only non-neural ectoderm, only neural ectoderm, or parts of both domains (Fig. 4B) already gives a rough approximation of the contour of the prospective neural tube material in the chick at stages 3d-4. The exclusively neural and non-neural domains are separated by a small gap that overlaps, as expected, the mixed-fate domains (Fig. 4A,B). The real boundary, if it is lineal, should lie somewhere along this gap, as exemplified by the line traced in Fig. 4C. The precision with which the neural/non-neural limit can be delineated with our approach is affected by the diameter of the grafts (i.e. might be increased with smaller grafts) and by the size of the areas of overlap or non-overlap obtained. However, the nature of the relevant regionalization process itself must be considered. It has been suggested that fate specification at the neural plate boundary may first occur aleatorily in a 'salt and pepper' pattern, under the control of proneurogenic genes (Selleck and Bronner-Fraser, 1995; Rubenstein et al., 1998; Brown and Storey, 2000). The 'salt and pepper' concept implies that 'fate-displaced' cells lying close to the forming boundary will segregate later in accordance with their specified fate, possibly as a result of differential adhesive properties. Close inspection of our material disclosed corroborating evidence for this hypothesis, as cases with grafts that closely approached the neural tube median roof from either side usually showed at least a few labeled cells dispersed in the opposite neural or non-neural domain (not shown). Our data, accordingly, do not negate but support some degree of interdigitation of the two fates at the border. Accordingly, a limit definition influenced by this idea might conceive the neural plate border to be represented by the whole border gap shown in our Fig. 4B. However, there is as well distinct evidence in our material that the actual border, even if bidimensional, must be thinner than this border gap (evidence collected in Fig. 4C).

We estimated as precisely as possible the boundary line depicted in Fig. 4C and Fig. 6D,E (see Results). Some extrapolation was needed across the least favorably determined border zones (Fig. 4C). At the rostral midline, for which we had more cases (Tables 1, 2), one graft, starting at 240 μm from the node, showed only a small contribution to rostral neural tissue and one case, whose distal edge was at 275 μm from the node, showed largely a neural fate, but had a small extraneural portion (Table 2). Moreover, grafts starting 270 or 280 μm apart from the node were wholly extraneural (Table 1). This reduces the maximum range for the width of the rostral border zone to a 240-270 μm interval. After considering comparable data from radial lines adjacent to this median area (Fig. 4C), we concluded, aiming for a reasonably smooth contour, that the midrostral border of the neural plate may be estimated to lie about 250 μm distant from the node periphery (Fig. 4C, Fig. 6E). For practical experimental purposes, this estimate and similar ones for other sectors of the boundary allow for a reasonable operating error of ±15 μm.

We thus recorded here both the border gap and our best estimate of a virtual line boundary (Fig. 4B,C, Fig. 6D,E). Researchers using the map for experimental embryology or for interpretation of gene expression patterns will select the border they feel is most significant for their purposes. Eventually, more conclusive evidence will accrue on the dimensions of the border area.

The radial extent of the neural plate clearly increases at each

side of the midline (Tables 1, 2) up to a maximum at the level of the prospective midbrain roof, which lies 475 μm away (radially) from the node (Fig. 4C, Fig. 6E). The radial dimension thereafter decreases caudalwards to a minimum value of 220 μm at prospective spinal cord levels (Fig. 4C, Fig. 6E). The slightly bi-lobed shape of the neural plate, with a central indentation, was unexpected, as no previous rendering of the rostral neural plate contour had given such a median indentation. However, the results on a shorter median dimension of neural tissue were clearly consistent with labeled neural plate border cells expressing the *Ganf* gene, a neural boundary marker (Fig. 9; Table 2) (Knoetgen et al., 1999).

We found few comparable data in the literature. The conclusions from Schoenwolf and Alvarez (Schoenwolf and Alvarez, 1991) and García-Martínez et al. (García-Martínez et al., 1993) revealed some discrepancies, with comparatively too large distances given for their 'boundary' grafts at the 0° and 90° lines. However, the data on the 45° radius given by these authors roughly agreed with ours. In the recent re-examination of these data by Lopez-Sanchez et al. (Lopez-Sanchez et al., 2001), the neural plate dimension at the 90° line is now coincident with ours, but there is still some discrepancy at the 0° line (border roughly 290 μm in front of the node).

A similar discrepancy exists as regards the extent and position of a postnodal part of the neural plate. This was placed by García-Martínez et al. (García-Martínez et al., 1993) 500-625 μm caudal to the node, and earlier authors gave postnodal lengths of 500-1000 μm (Spratt, 1952; Rudnick, 1938; Schoenwolf et al., 1989b). The fate map of García-Martínez et al. (García-Martínez et al., 1993) also suggested that the postnodal extent of the prospective neural plate was larger laterally than close to the primitive line [not corroborated by our data and largely corrected by Lopez-Sanchez et al. (Lopez-Sanchez et al., 2001)]. Other authors supporting a postnodal neuroectodermal portion are Rawles (Rawles, 1936), Rudnick (Rudnick, 1944), Rosenquist (Rosenquist, 1966) and Vakaet (Vakaet, 1984). However, Bortier and Vakaet (Bortier and Vakaet, 1992) strictly denied the existence of any postnodal representation of the neural plate at comparable stages. Our data indicate (Fig. 4A-C; Tables 1-3) that the neural plate descends at least 230 μm behind the node, and has a similar mediolateral extent – 220 μm (Fig. 6E). Several grafts placed more caudally produced only mesodermal and endodermal derivatives (Fig. 4B, Fig. 6D,E). Some of the discrepancies might be explained by staging inaccuracies.

Our analysis obviously refers to the caudalmost neural tissue developed into histologically characteristic spinal cord or neural canal at stages 9-11. This is only a part of the definitive spinal cord. In principle, stem cells can exist within the presently mapped anlage, whose subsequent clonal expansion can extend the spinal cord caudally (Gont et al., 1993; Catala et al., 1995; Catala et al., 1996; Charrier et al., 1999; Nicolas et al., 1996; Mathis et al., 1999; Mathis and Nicolas, 2000a; Mathis and Nicolas, 2000b). However, we cannot discount with the present data that some caudal tissue classified here as 'non-neural' at stages 9-11 may be induced to adopt a neural fate later on (Schoenwolf, 1992), as neural inducing molecules are continually expressed at the regressing node (Doniach, 1995; Doniach and Musci, 1995; Storey et al., 1998; Streit and Stern, 1999). Full resolution of this question would need extending the survival of the experimental specimens until stages in which the spinal cord is complete.

Rostrocaudal divisions of the neural plate

Previous fate maps of the avian neural plate gave only limited attention to the experimental definition of prospective rostrocaudal regions of the neural tube. This issue is complicated by large morphogenetic changes affecting the apparent topography of the respective derivatives, as well as by relative scarcity of morphological landmarks that serve to determine rostrocaudal positions unambiguously. While some gene expression patterns are routinely used to assess rostrocaudal specification in neural induction experiments, few of these markers are expressed in the early neural plate, or have been tested for correlation with the assumed prospective fate. It is often uncertain whether the earliest expression of a gene is topographically fixed in correlation with fate, as opposed, for example, to expression domains changing as development proceeds (Gardner et al., 1988; Hollyday et al., 1995; Bally-Cuif et al., 1995; Shamin and Mason, 1998; Goriely et al., 1999; Hidalgo-Sánchez et al., 1999).

In addition, there have been recent changes in the concept of some rostrocaudal limits, as a result of fate mapping studies in the closed neural tube. For example, the isthmomesencephalic boundary is now known to be placed inside what was thought to be midbrain previously (Martínez and Alvarado-Mallart, 1989; Hallonet et al., 1990; Marín and Puelles, 1994; Puelles et al., 1996; Millet et al., 1999) and the medullospinal boundary was recently relocated across the fifth somite (Cambronero and Puelles, 2000).

Earlier authors have variously separated the prospective forebrain, midbrain, hindbrain and spinal cord regions by lines that alternatively (1) diverge from the node (Rudnick, 1944), (2) are all transverse to the axis and parallel to each other (Bortier and Vakaet, 1992), or (3) show a hybrid pattern, where rostral lines are orthogonal to the midline at prenodal levels, whereas more caudal lines diverge from the node caudalwards (Wetzel, 1929; Wetzel, 1936; Spratt, 1952; Rudnick, 1961). The maps by Schoenwolf et al. (Schoenwolf et al., 1989a), Schoenwolf and Alvarez (Schoenwolf and Alvarez, 1991), García-Martínez et al. (García-Martínez et al., 1993) and Lopez-Sanchez et al. (Lopez-Sanchez et al., 2001) did not include conclusions in this respect.

We approached this problem through comparison of a number of different cases, which overlapped in various ways across the transverse boundary areas. The sets of grafts which could be confidently interpreted as labeling mainly either the forebrain, midbrain, hindbrain or spinal cord (Fig. 5) showed areas of partial intersection (Fig. 6A). Note that the dimensions of these graphic overlap zones reflect the size of the component grafts, but only a small part of the derived cells of each graft lie at the prospective boundaries. Therefore, these overlap zones are significant as indicators of the overall position of the boundaries, but not of their width at stage 4. Our virtual prospective transverse limits therefore were traced as lines roughly bisecting these areas of overlap (Fig. 6A,D). Smaller grafts or dye injections might explore the possible width of these borders, in conjunction with analysis of region-specific gene expression patterns.

The resulting prospective transverse subdivisions diverge uniformly from the node (Rudnick, 1944). The forebrain is a

large wedge-shaped area and measures at each side from the midline 70 μm paranodally and 350 μm peripherally. The midbrain, hindbrain and spinal cord regions are also wedge shaped and their comparable rostrocaudal dimensions measure roughly 60 μm paranodally and 200 μm peripherally (see Table 4). The main novelty in these results possibly lies in the considerable obliquity of the midbrain-forebrain boundary, which projects the dorsal midbrain into the lateralmost aspect of the apparent rostral part of the neural plate. This result is unambiguously supported by cases such as L-114b (Fig. 5D and inset). The other more caudal boundaries also are oblique rostralwards, in contrast to all earlier formulations in the chick. Such early obliquity (which is presumably redressed later, as elongation of the axis proceeds) agrees with the even stronger obliquity of the same limits fate-mapped in the unincubated chicken blastoderm (Callebaut et al., 1996) or in frogs at mid-blastula (Jacobson, 1982). Expression of the gene *Irx2* (a hindbrain marker) in the chick neural plate was reported as changing from an early prenodal position to a later postnodal one (Goriely et al., 1999), consistent with the presumed evolution of early hindbrain fate shown in our map.

Longitudinal partition of the neural plate

Our suggested division of the neural plate into prospective basal and alar longitudinal components is tentative, as it referred a priori to an arbitrary line separating the ventral third from the dorsal two thirds of the closed neural tube at stages 9-11. This initial disproportion is known to increase at later stages, which is due to the differential proliferative dynamics of these territories. Following the rationale explained above for transversal boundaries, we approximated the position of the alar/basal limit in the fate map by a line bisecting the set of intersections between grafts classified as contributing to such roughly delimited ‘alar’ or ‘basal’ domains (Fig. 6C). Our data do not reveal whether this limit has a width. The resulting schema mainly serves to highlight a larger expanse of alar plate in the forebrain and midbrain, while there is a relatively smaller alar plate component at hindbrain and spinal cord levels (Fig. 6D).

The floor plate

Some of our data bear upon the origin of the floor plate. Previous studies by Schoenwolf et al. (Schoenwolf et al., 1989a; Schoenwolf et al., 1989b) compared grafts placed just rostral or lateral to the node and concluded that floor plate tissue is produced only rostral to the node. However, some of our grafts placed lateral to the node or primitive line distinctly contributed cells to the floor plate at stages 9-11 (Fig. 8J-L). Comparing these results with other cases which labeled only the basal plate at similar levels, we estimated that the width of a prospective floor plate domain cannot be larger than 15-20 μm (Fig. 6D). This dimension roughly coincides with our estimate of the resolution limit in our data set, which necessarily makes our floor plate representation in Fig. 6D tentative. Nevertheless, there is the fact that a floor plate fate can be obtained lateral to the node and primitive line (Fig. 8J-L). We attribute to the larger number of cases in the present set of experiments, and to their inherent small variability, that we actually detected this small contribution, thus possibly explaining the negative results of Schoenwolf et al. (Schoenwolf et al., 1989a).

Selleck and Stern (Selleck and Stern, 1991) fate-mapped the node itself in the chick at several stages, including stage 4. While most of the prospective notocordal tissue was found in a rostromedial sector of the node, additional contributions were also recorded from more caudolateral sectors. Owing to the intimate correlation of prospective notochord and floor plate material in vertebrates, these data are also consistent with the existence of small caudolateral wings of the avian ‘notoplate’ (Jacobson, 1994), as suggested in our fate map (Fig. 6D). In this context, it seems tenable, as well as parsimonious in terms of fate determining mechanisms, to think that the laterally placed floor plate domain may be topologically continuous with the as yet ungastrulated prospective mesoderm/endoderm (similarly as the median prenodal material is continuous with the notochord). The well-known formation of elongated axial clonal derivatives from nodal or prenodal primordia (Lopez-Sanchez et al., 2001) does not, in principle, exclude that other clones may be added further back from laterally placed precursors. The hypothetic caudolateral wings of floor plate would separate the notoplate-mesoderm border from the basal plate, whereas alar plate would limit selectively with prospective non-neural ectoderm (see Tables 2 and 3 for data consistent with this assumption). That was our rationale for interpreting case L-56 and tracing the wing-shaped tentative basal-floor boundary as shown in Fig. 6D.

The eye field

There is limited information in the literature on the location and size of the eye fields in the early chick neural plate (Butler, 1935; Spratt, 1940; Rudnick, 1944; Romanoff, 1960; Couly and Le Douarin, 1987). We addressed these points at stages 3d-4 as regards the optic vesicles identified at stages 9-11. Our results need to be interpreted with caution, because we still ignore how much of these stage 9-11 ‘optic vesicles’ actually contribute material to the definitive eyes. Partial results of Smith-Fernández et al. (Smith-Fernández et al., 1998), from a study exploring the location of prospective telencephalic primordia at stage 9, revealed that grafts invading the dorsal aspect of the ‘optic vesicles’ contribute derivatives to the telencephalon. Unfortunately, the authors did not mention whether these grafts also contributed to the eye itself, so that the actual boundary of the presumptive eye at stage 9 remains unclear. Moreover, there is no strong criterion for identifying the chiasmatic region at stages 9-11, as the optic chiasm barely starts to form at stage 24. We therefore tentatively took the whole evaginating bulge to be prospective eye.

Our data locate the eye field between the 20° and 40° lines anteroposteriorly, at a distance of 160 μm to 320 μm from the border of the node, consistent with the position and dimensions of case L-82, which labeled most of the evaginated optic vesicle (Fig. 5B,G,H; see Table 2). Fig. 6B also collects other relevant cases, comprising grafts that labeled tissue just outside the optic vesicle (light blue-shaded), and cases that partially penetrated it (yellow-shaded; see Tables 2, 3). Overlaps between these sets (green) were interpreted as lying outside the eye field. These data allowed us to draw a tentative contour of the eye field, which agrees with more precise eye field results from the stage 8 chick forebrain fate map created by Cobos et al. (Cobos et al., 2001), as well as with earlier data by Couly and LeDouarin (Couly and Le Douarin, 1987).

Our observation of strictly conserved laterality of eye

derivatives (as well as of all forebrain in general) suggests that any earlier cell-intercalation phenomena that might cause precocious mixing of right and left clonal derivatives across a median eye field (or a median forebrain field) (Jacobson, 1982) would have ended in the chick at initial neural plate stages.

Neural plate border in relationship with gene expression data

Recent literature on chick neural plate stages reports a number of genes that are expressed differentially in the neural/non-neural ectoderm continuum. Several expression domains surrounding the node are thought to label the neural plate: *Otx2* (Bally-Cuif et al., 1995); *Sox2/3 and Sox21* (Rex et al., 1997a; Rex et al., 1997b); *Gsx* (Lemaire et al., 1997); *Six3* (Bovolenta et al., 1998); *Gbx2* (Shamin and Mason, 1998); *Ganf* (Knoetgen et al., 1999); *Tbr2* (Bulfone et al., 1999); *Rax/rx* (Ohuchi et al., 1999); *Lmx1* (Yuan and Schoenwolf, 1999); *Frzb1* (Baranski et al., 2000); *Plato* (Lawson et al., 2000). By contrast, genes expressed in the area pellucida, surrounding a central area around the node, have been conceived as markers of prospective 'non-neural' territory: *Dlx5* (Ferrari et al., 1995; Pera et al., 1999; Borghjid and Siddiqui, 2000); *Crescent* (Pfeffer et al., 1997); *BMP4*/*BMP7* (Liem et al., 1995; Watanabe and Le Douarin, 1996; Schultheiss et al., 1997; Lemaire and Kessell, 1997); *Smad6* (Yamada et al., 1999). In general, these gene patterns have not been correlated directly with fate-mapping data, and in most cases they have not been compared with each other. Gene expressions observed at early embryonic stages may be dynamic in topography, unless correlations with fate-map data suggest otherwise. However, previous fate maps were divergent in their conclusions about neural plate dimensions, so that the issue whether any of these postulated 'neural' or 'non-neural' genes have a fixed pattern and actually identify the prospective boundary of the neural plate clearly remained open. We comment on our present expression data on *Otx2*, *Dlx5*, *Plato*, *Sox2* and *Ganf*, and later consider briefly other relevant data in the literature. The question is whether the experimentally mapped neural plate boundary coincides with any of these molecular signals.

We addressed in control experiments the issue of whether map measurements (graft distance from the node on the living embryos) suffer distortions during fixation and processing for in situ hybridization (in order to be able to compare meaningfully with literature and own data on gene expressions). We were not aware of any previous data on this aspect. We found only minimal distortion – a 3% retraction – with the procedures employed by us. Any comparability errors arising from this distortion would, accordingly, be within the range of the resolution limits of this fate map (±17.5 μm; i.e. 3% of 250 μm is 7 μm).

We thus re-examined the early expression of some markers (*Ganf*, *Plato*, *Sox2*, *Otx2* and *Dlx5*), to evaluate their correlation with the fate map described in this work, corrected for 3% retraction. The *Ganf* signal at stage 4 mapped across the rostral ridge of the plate (Fig. 9A). At stages 9-11 (Knoetgen et al., 1999), it clearly overlaps with cells derived from the rostromedian indented border of the neural plate, as we also verified experimentally (Fig. 9F).

Neither *Plato* (Lawson et al., 2000) (Fig. 10A) nor *Sox2* expression (Rex et al., 1997a) (Fig.10B) completely delineate the mapped neural plate shape, but their transcripts are largely restricted to the neural plate area, and at the midline both reach from the node to the prospective anterior boundary. Our study of the *Otx2* domain at stage 4 suggests that it completely overlaps the mapped neural plate, but also extends somewhat into the surrounding non-neural ectoderm, particularly mid-rostrally and laterocaudally, more so than occurs with *Sox2* (Fig. 10B,C). *Dlx5* is thought to represent a marker of prospective non-neural epiblast (Pera et al., 1999). In our hands, *Dlx5* expression lies wholly outside the mapped border of the neural plate, and appears to be slightly outside the peripheral border of *Otx2* (Fig. 10D).

Only *Ganf*, *Plato* and *Sox2* show a topography that approximates the size and shape of the mapped neural plate, though none of them labels it entirely and homogeneously, or excludes some expression in neighboring median or laterocaudal non-neural ectoderm. Several other genes reported in the literature (*Tbr2*, *Sox3*, *Frzb1*, *Sox21*) and unpublished (*Sox3*; P. F.-G., L. R.-G., V. G.-D., I. S. A. and L. Puelles, unpublished) also have expression domains at stage 4 that cover partly or totally the neural plate, variously extending as well into non-neural areas.

We therefore conclude that several genes that are expressed shortly after neural induction correlate at least roughly with the fate map described, and particularly with its midrostral border. However, various sorts of differences, difficult to evaluate at present, seem to exist in the precise topography of the borders of expression of the different genes relative to the AP and DV neural plate dimensions mapped at stages 3d/4. For example, the mapped rostral indentation of the prospective forebrain primordium is not delineated by most of the studied genes, presumably leaving a molecularly distinct median triangular space for the prospective adenohypophysis (Couly and Le Douarin, 1985; Couly and Le Douarin, 1987; Rubenstein et al., 1998; Cobos et al., 2001). Curiously, expression of *Bmp7* in the mes-endoderm layer under the epiblast seems to fill specifically the triangular space under the median non-neural indentation (Nieto, 2001).

Work is supported by EEC contract ERB-FMRX-CT96-0065, Séneca Foundation grant PB/25/FS/99 and DGES grant PB98-0397 (L. P.); grant DGES PB97-0371 and grant from the Junta de Extremadura (I. S. A.); grant from the Junta de Extremadura (L. R.-G.); and by a Spanish MEC fellowship (V. G.-D.). The collaboration of V. García-Martínez and C. López-Sánchez is gratefully acknowledged. M. Kessel, A. Simeone, P. J. Scotting, J. L. R. Rubenstein and G. C. Schoenwolf kindly provided gene probes.

REFERENCES

Alvarez, I. S. and Schoenwolf, G. C. (1991). Patterns of neuroepithelial cell rearrangement during avian neurulation are determined prior to nothochordal inductive interactions. *Dev. Biol.* **143**, 78-92.

Bally-Cuif, L., Gulisano, M., Broccoli, V. and Boncinelli, E. (1995). c-Otx-2 is expressed in two different phases of gastrulation and is sensitive to retinoic acid treatment in the chick embryo. *Mech. Dev.* **49**, 49-63.

Baranski, M., Berdougo, E., Sandler, J. S., Darnell, D. K. and Burrus, L. W. (2000). The dynamic expression pattern of frzb-1 suggests multiple roles in chick development. *Dev. Biol.* **217**, 25-41.

Borghjid, S. and Siddiqui, M. A. (2000). Chick homeobox gene cDlx expression demarcates the forebrain anlage, indicating the onset of forebrain regional specification at gastrulation. *Dev. Neurosci.* **22**, 183-196.

Bortier, H. and Vakaet, L. (1992). Fate mapping the neural plate and the intraembryonic mesoblast in the upper layer of the chicken blastoderm with xenografting and time-lapse videography. *Development* **Suppl.**, 93-97.

Bovolenta, P., Mallamaci, A., Puelles, L. and Boncinelli, E. (1998). Expression pattern of cSix3, a member of the Six/sine oculis family of transcription factors. *Mech. Dev*. **70**, 201-203.

Brown, J. M. and Storey, K. G. (2000). A region of the vertebrate neural plate in which neighbouring cells can adopt neural or epidermal. *Curr. Biol*. **10**, 869-872.

Bulfone, A., Martinez, S., Marigo, V., Campanella, M., Basile, A., Quaderi, N., Gattuso, C., Rubenstein, J. L. and Ballabio, A. (1999). Expression pattern of the Tbr2 (Eomesodermin) gene during mouse and chick brain development. *Mech. Dev.* **84**, 133-138.

Butler, E. (1935). The development capacity of regions of the unincubated chick blastoderm as tested in choriod-allantoic grafts. *J. Exp. Zool*. **70**, 387-338.

Callebaut, M., van Nueten, E., Bortier, H., Harrisson, F. and van Nassauw, L. (1996). Map of the Anlage fields in the avian unincubated blastoderm. *Eur. J. Morphol*. **34**, 347-361.

Cambronero, F. and Puelles, L. (2000). Rostrocaudal nuclear relationships in the avian medulla oblongata: a fate map with quail chick chimeras. *J. Comp. Neurol*. **427**, 522-545.

Catala, M., Teillet, M. A. and le Douarin, N. M. (1995). Organization and development of the tail bud analyzed with the quail-chick chimaera system. *Mech. Dev.* **51**, 51-65.

Catala, M., Teillet, M. A., de Robertis, E. M. and le Douarin, N. M. (1996). A spinal cord fate map in the avian embryo: while regressing, Hensen's node lays down the notochord and floor plate thus joining the spinal cord lateral walls. *Development* **122**, 2599-2610.

Charrier, J. B., Teillet, M. A., Lapointe, F. and le Douarin, N. M. (1999). Defining subregions of Hensen's node essential for caudalward movement, midline development and cell survival. *Development* **126**, 4771-4783.

Cobos, I., Shimamura, K., Rubenstein, J. L. R., Martinez, S. and Puelles, L. (2001). Fate map of the avian anterior forebrain at the 4 somite stage, based on the analysis of quail-chick chimeras. *Dev. Biol*. **239**, 46-67.

Couly, G. F. and Le Douarin, N. M. (1985). Mapping of the early neural primordium in quail-chick chimeras. I. Developmental relationships between placodes, facial ectoderm, and prosencephalon. *Dev. Biol.* **110**, 422-439.

Couly, G. F. and Le Douarin, N. M. (1987). Mapping of the early neural primordium in quail-chick chimeras. II. The prosencephalic neural plate and neural folds: implications for the genesis of cephalic human congenital abnormalities. *Dev. Biol*. **120**, 198-214.

Darnell, D. K., Stark, M. R. and Schoenwolf, G. C. (1999). Timing and cell interactions underlying neural induction in the chick embryo. *Development* **126**, 2505-2514.

Darnell, D. K., García-Martínez, V., López-Sánchez, C., Yuan, S. and Schoenwolf, G. C. (2000). Dynamic labelling techniques for fate mapping, testing cell commitment, and following living cells in avian embryos. In *Methods in Molecular Biology, Vol. 135: Developmental Biology Protocols, Vol. I* (ed. R. S. Tuan and C. W. Lo), pp 305-321. Totowa, NJ: Humana Press.

Doniach, T. (1995). Basic FGF as an inducer of anteroposterior neural pattern. *Cell* **83**, 1067-1070.

Doniach, T. and Musci, T. J. (1995). Induction of anteroposterior neural pattern in Xenopus: evidence for a quantitative mechanism, *Mech. Dev*. **53**, 403-413.

Fernández-Garre, P., Rodríguez-Gallardo, L., Alvarez, I. S. and Puelles, L. (2002). A neural plate fate map at stage HH4 in the chick: Methodology and preliminary data. *Brain Res. Bull.* **57**, 293-295.

Ferrari, D., Sumoy, L., Gannon, J., Sun, H., Brown, A. M., Upholt, W. B. and Kosher, R. A. (1995). The expression pattern of the Distal-less homeobox-containing gene Dlx-5 in the developing chick limb bud suggests its involvement in apical ectodermal ridge activity, pattern formation, and cartilage differentiation. *Mech. Dev.* **52**, 257-264.

García-Martínez, V., Alvarez, I. S. and Schoenwolf, G. C. (1993). Locations of the ectodermal and nonectodermal subdivisions of the epiblast at stages 3 and 4 of avian gastrulation and neurulation. *J. Exp. Zool*. **267**, 431-446.

Gardner, C. A., Darnell, D. K., Poole, S. J., Ordahl, C. P. and Barald, K. F. (1988). Expression of an engrailed-like gene during development of the early embryonic chick nervous system. *J. Neurosci. Res.* **21**, 426-437.

Gont, L. K., Steinbeisser, H., Blumberg, B. and de Robertis, E. M. (1993). Tail formation as a continuation of gastrulation: the multiple cell populations of the Xenopus tailbud derive from the late blastopore lip. *Development* **119**, 991-1004.

Goriely, A., Diez del Corral, R. and Storey, K. G. (1999). c-Irx2 expression reveals an early subdivision of the neural plate in the chick embryo. *Mech. Dev.* **87**, 203-206.

Hallonet, M. E., Teillet, M. A. and le Douarin, N. M. (1990). A new approach to the development of the cerebellum provided by the quail-chick marker system, *Development* **108**, 19-31.

Hamburger, V. and Hamilton, H. L. (1951). A series of normal stages in the development of the chick embryo. *J. Morphol.* **88**, 49-92.

Hatada, Y. and Stern, C. D. (1994). A fate map of the epiblast of the early chick embryo. *Development* **120**, 2879-2889.

Hauptmann, G. and Gerster, T. (2000). Regulatory gene expression patterns reveal transverse and longitudinal subdivisions of the embryonic zebrafish forebrain. *Mech. Dev.* **91**, 105-118.

Hidalgo-Sanchez, M., Simeone, A. and Alvarado-Mallart, R. M. (1999). Fgf8 and Gbx2 induction concomitant with Otx2 repression is correlated with midbrain-hindbrain fate of caudal prosencephalon. *Development* **126**, 3191-3203.

Hollyday, M., McMahon, J. A. and McMahon, A. P. (1995). Wnt expression patterns in chick embryo nervous system. *Mech. Dev.* **52**, 9-25.

Jacobson, A. G. (1994). Normal neurulation in amphibians. *Ciba Found. Symp.* **181**, 6-24.

Jacobson, M. (1982). Origins of the nervous system in amphibians. In *Neuronal Development* (ed. N. C. Spitzer), pp 45-99. New York: Plenum Press.

Knoetgen, H., Viebahn, C. and Kessel, M. (1999). Head induction in the chick by primitive endoderm of mammalian, but not avian origin. *Development* **126**, 815-825.

Lawson, A., Colas, J. F. and Schoenwolf, G. C. (2000). Ectodermal markers delineate the neural fold interface during avian neurulation. *Anat. Rec.* **260**, 106-109.

Lemaire, L. and Kessel, M. (1997). Gastrulation and homeobox genes in chick embryos. *Mech. Dev.* **67**, 3-16.

Lemaire, L., Roeser, T., Izpisua-Belmonte, J. C. and Kessel, M. (1997). Segregating expression domains of two goosecoid genes during the transition from gastrulation to neurulation in chick embryos. *Development* **124**, 1443-1452.

Liem, K. F., Tremml, G., Roelink, H. and Jessell, T. M. (1995). Dorsal differentiation of neural plate cells induced by BMP-mediated signals from epidermal ectoderm. *Cell* **82**, 969-979.

Lopez-Sanchez, C., García-Martinez, V. and Schoenwolf, G. (2001). Localization of cells of the prospective neural plate, heart and somites within the primitive streak and epiblast of avian embryos at intermediate primitive-streak stages. *Cells Tiss. Org.* **169**, 334-346.

Marín, F. and Puelles, L. (1994). Patterning of the embryonic avian midbrain after experimental inversions: a polarizing activity from the isthmus. *Dev. Biol*. **163**, 19-37.

Martínez, S. and Alvarado-Mallart, R. M. (1989). Transplanted mesencephalic quail cells colonize selectively all primary visual nuclei of chick diencephalon: a study using heterotopic transplants. *Dev. Brain Res.* **47**, 263-274.

Mathis, L. and Nicolas, J. F. (2000a). Different clonal dispersion in the rostral and caudal mouse central nervous system. *Development* **127**, 1277-1290.

Mathis, L. and Nicolas, J. F. (2000b). Clonal organization in the postnatal mouse central nervous system is prefigured in the embryonic neuroepithelium. *Dev. Dyn.* **219**, 277-281.

Mathis, L., Sieur, J., Voiculescu, O., Charnay, P. and Nicolas, J. F. (1999). Successive patterns of clonal cell dispersion in relation to neuromeric subdivision in the mouse neuroepithelium. *Development* **126**, 4095-4106.

Millet, S., Campbell, K., Epstein, D. J., Losos, K., Harris, E. and Joyner, A. L. (1999). A role for Gbx2 in repression of Otx2 and positioning the mid/hindbrain organizer. *Nature* **401**, 161-164.

New, D. A. T. (1955). A new technique for the cultivation of the chick embryo in vitro. *J. Embryol. Exp. Morphol.* **3**, 326-331.

Nicolas, J. F., Mathis, L., Bonnerot, C. and Saurin, W. (1996). Evidence in the mouse for self-renewing stem cells in the formation of a segmented longitudinal structure, the myotome. *Development* **122**, 2933-2946.

Nicolet, G. (1970). An autoradiographic study of the presumptive fate of the primitive streak in chick embryos. *J. Embryol. Exp. Morphol.* **23**, 79-108.

Nicolet, G. (1971). Avian gastrulation. *Adv. Morphogen.* **9**, 231-262.

Nieto, M. A. (2001) The early steps of neural crest development. *Mech. Dev.* **105**, 27-35.

Ohuchi, H., Tomonari, S., Itoh, H., Mikawa, T. and Noji, S. (1999). Identification of chick rax/rx genes with overlapping patterns of expression during early eye and brain development. *Mech. Dev.* **85**, 193-195.

Pera, E., Stein, S. and Kessel, M. (1999). Ectodermal patterning in the avian embryo: epidermis versus neural plate. *Development* **126**, 63-73.

Pfeffer, P. L., de Robertis, E. M. and Izpisua-Belmonte, J. C. (1997). Crescent, a novel chick gene encoding a Frizzled-like cysteine-rich domain, is expressed in anterior regions during early embryogenesis. *Int. J. Dev. Biol.* **41**, 449-458.

Puelles, L., Amat, J. A. and Martinez-de-la-Torre, M. (1987). Segment-related, mosaic neurogenetic pattern in the forebrain and mesencephalon of early chick embryos: I. Topography of AChE-positive neuroblasts up to stage HH18. *J. Comp. Neurol.* **266**, 247-268.

Puelles, L. and Rubenstein, J. L. (1993). Expression patterns of homeobox and other putative regulatory genes in the embryonic mouse forebrain suggest a neuromeric organitation. *Trends. Neurosci.* **16**, 472-479.

Puelles, L., Marín, F., Martínez-de-la-Torre, M. and Martínez, S. (1996) The midbrain-hindbrain junction: a model system for brain regionalization through morphogenetic neuroepithelial interactions. In *Mammalian Development* (ed. P. Lonai), pp 173-197. Amsterdam: Harwood Academic Publishers.

Rawles, M. E. (1936). A study in the localization of organ-forming areas in the chick blastoderm of the head-process stage. *J. Exp. Zool.* **72**, 271-315.

Rex, M., Orme, A., Uwanogho, D., Tointon, K., Wigmore, P. M., Sharpe, P. T. and Scotting, P. J. (1997a). Dynamic expression of chicken Sox2 and Sox3 genes in ectoderm induced to form neural tissue. *Dev. Dyn.* **209**, 323-332.

Rex, M., Uwanogho, D. A., Orme, A., Scotting, P. J. and Sharpe, P. T. (1997b). cSox21 exhibits a complex and dynamic pattern of transcription during embryonic development of the chick central nervous system. *Mech. Dev.* **66**, 39-53.

Romanoff, A. L. (1960). *The Avian Embryo Structural and Funcional Development.* New York: MacMillan.

Rosenquist, G. C. (1966). A radioautographic study of labeled grafts in the chick blastoderm. Development from primitive-streak stages to stage 12. *Contrib. Embryol. Carnegie Inst.* **38**, 73-110.

Rubenstein, J. L., Shimamura, K., Martinez, S. and Puelles, L. (1998). Regionalization of the prosencephalic neural plate. *Annu. Rev. Neurosci.* **21**, 445-477.

Rudnick, D. (1938). Contribution to the problem of neurogenic potency in post-nodal isolates from chick blastoderms. *J. Exp. Zool.* **78**, 369-383.

Rudnick, D. (1944). Early history and mechanics of the chick blastoderm. A review. *Quart. Rev. Biol.* **19**, 187-212.

Rudnick, D. (1961). Teleosts and Birds. In *Analysis of Development* (ed. P. A. Willier, P. Weiss and V. Hamburger). pp. 297-314. Philadelphia: Saunders.

Schoenwolf, G. C. (1988). Microsurgical analyses of avian neurulation: separation of medial and lateral tissues. *J. Comp. Neurol.* **276**, 498-597.

Schoenwolf, G. C. (1991). Cell movements driving neurulation in avian embryos. *Development* **Suppl. 2**, 157-168.

Schoenwolf, G. C. (1992). Morphological and mapping studies of the paranodal and postnodal levels of the neural plate during chick neurulation. *Anat. Rec.* **233**, 281-290.

Schoenwolf, G. C. and Alvarez, I. S. (1989). Roles of neuroepithelial cell rearrangement and division in shaping of the avian neural plate. *Development* **106**, 427-439.

Schoenwolf, G. C. and Alvarez, I. S. (1991). Specification of neurepithelium and surface epithelium in avian transplantation chimeras. *Development* **112**, 713-722.

Schoenwolf, G. C., Bortier, H. and Vakaet, L. (1989a). Fate mapping the avian neural plate with quail/chick chimeras: origin of prospective median wedge cells. *J. Exp. Zool.* **249**, 271-278.

Schoenwolf, G. C., Everaert, S., Bortier, H. and Vakaet, L. (1989b). Neural plate- and neural tube-forming potential of isolated epiblast areas in avian embryos. *Anat. Embryol.* **179**, 541-549.

Schoenwolf, G. C., Garcia-Martinez, V. and Dias, M. S. (1992). Mesoderm movement and fate during avian gastrulation and neurulation. *Dev. Dyn.* **193**, 235-248.

Schoenwolf, G. C. and Sheard, P. (1990). Fate mapping the avian epiblast with focal injections of a fluorescent-histochemical marker: ectodermal derivates. *J. Exp. Zool.* **255**, 323-339.

Schultheiss, T. M., Burch, J. B. and Lassar, A. B. (1997). A role for bone morphogenetic proteins in the induction of cardiac myogenesis. *Genes Dev.* **11**, 451-462.

Selleck, M. A. and Bronner-Fraser, M. (1995). Origins of the avian neural crest: the role of neural plate-epidermal interactions. *Development* **121**, 525-538.

Selleck, M. A. and Stern, C. D. (1991). Fate mapping and cell lineage analysis of Hensen's node in the chick embryo. *Development* **112**, 615-626.

Shamim, H. and Mason, I. (1998). Expression of Gbx-2 during early development of the chick embryo. *Mech. Dev.* **76**, 157-159.

Shimamura, K., Hirano, S., McMahon, A. P. and Takeichi, M. (1994). Wnt-1-dependent regulation of local E-cadherin and _N-catenin expression in the embryonic mouse brain. *Development* **120**, 2225-2234.

Shimamura, K., Hartigan, D. J., Martinez, S., Puelles, L. and Rubenstein, J. L. (1995). Longitudinal organization of the anterior neural plate and neural tube. *Development* **121**, 3923-3933.

Shimamura, K., Martinez, S., Puelles, L. and Rubenstein, J. L. (1997). Patterns of gene expression in the neural plate and neural tube subdivide the embryonic forebrain into transverse and longitudinal domains. *Dev. Neurosci.* **19**, 88-96.

Smith, J. L. and Schoenwolf, G. (1987). Cell cycle and neuroepithelial cell shape during bending of the chick neural plate. *Anat. Rec.* **218**, 196-206.

Smith-Fernández, A., Pieau, C., Repérant, J., Boncinelli, E. and Wassef, M. (1998). Expression of the Emx-1 and Dlx-1 homeobox genes define three molecularly distinct domains in the telencephalon of mouse, chick, turtle and frog embryos: implications for the evolution of telencephalic subdivisions in amniotes. *Development* **125**, 2099-2111.

Spratt, N. T. (1940). An in vitro analysis of the organization of the eye-forming area in the early chick blastoderm. *J. Exp. Zool.* **85**, 171-209.

Spratt, N. T. (1952). Localization of the prospective neural plate in the early chick blastoderm. *J. Exp. Zool.* **120**, 109-130.

Stern, C. D. and Ireland, G. W. (1981). An integrated experimental study of endoderm formation in avian embryos. *Anat. Embryol.* **163**, 245-263.

Storey, K. G., Goriely, A., Sargent, C. M., Brown, J. M., Burns, H. D., Abud, H. M. and Heath, J. K. (1998). Early posterior neural tissue is induced by FGF in the chick embryo. *Development* **125**, 473-484.

Streit, A. and Stern, C. D. (1999). Establishment and maintenance of the border of the neural plate in the chick: involvement of FGF and BMP activity. *Mech. Dev.* **82**, 51-66.

Vakaet, L. (1984). Early development of birds. In *Chimeras in Developmental Biology* (ed. N. Le Douarin and A. McLaren), pp. 71-88. London: Academic Press.

Watanabe, Y. and Le Douarin, N. M. (1996). A role for BMP-4 in the development of subcutaneous cartilage. *Mech. Dev.* **57**, 69-78.

Wetzel, R. (1929). Untersuchungen am Hühnchen. Die Entwicklung des Keims während der erste beiden Bruttage. *Arch. Entwicklungsmech. Organ.* **119**, 188-321.

Wetzel, R. (1936). Primitivstreifen und Urkörper nach Störungsversuchen am 1-2 Tage bebrüteten Hühnchen. *Arch. Entwicklungsmech. Organ.* **134**, 357-465.

Yamada, M., Szendro, P. I., Prokscha, A., Schwartz, R. J. and Eichele, G. (1999). Evidence for a role of Smad6 in chick cardiac development. *Dev. Biol.* **215**, 48-61.

Yuan, S. and Schoenwolf, G. C. (1999). The spatial and temporal pattern of C-Lmx1 expression in the neuroectoderm during chick neurulation. *Mech. Dev.* **88**, 243-247.